LOW-LOSS GROUNDED ELEVATED COPLANAR WAVE-GUIDE FOR SUB-MILLIMETER WAVE MMIC APPLICATIONS

F. Aghamoradi[*], I. McGregor, S. Roy, and K. Elgaid

Electronics & Electrical Engineering Department, University of Glasgow, United Kingdom

Abstract—A new type of elevated coplanar waveguide structure is described which uses airbridge technology to suspend CPW traces above a ground plane resting on a high permittivity substrate. The transmission line is effectively shielded from the substrate and is equivalent to conductor backed CPW with an extremely thin, air substrate. It is, therefore, insensitive to parasitic substrate effects such as surface waves and the effect of dielectric loss tangent. In comparison with other forms of CPW with typical lateral dimensions, the structure exhibits no high frequency roll-off at frequencies of around 240 GHz and above. Measured results show 2.5 dB/mm insertion loss at 320 GHz for a 51 Ω line. In order to demonstrate the performance of the new line at mm-wave frequencies, several passive components have been fabricated, measured and their performance compared with CPW counterparts. The experimental results, which are in close agreement with simulation results, for short and open circuited matching stubs, and band-pass and band-stop filters, clearly show improvements in terms of loss and in the characteristics of the frequency response. Also, in order to make some qualitative assessment of the variation in performance with elevation, results for elevations of 6 μm and 13 μm are compared. Low loss and a simple, MMIC compatible, fabrication process make grounded elevated CPW a promising transmission media for MMIC applications at the very high end of the millimeter-wave frequency spectrum.

* Corresponding author: Fatemeh Aghamoradi (l.aghamoradi@gmail.com).

1. INTRODUCTION

Transmission Lines are the most basic components of MMIC designs and achieving a low-loss, MMIC compatible, transmission line can be a challenge at high mm-wave frequencies. CPW structures are, generally, the preferred choice for mm-wave applications due, in part, to the simplicity of grounding semiconductor devices without the need of vias [1–3] and with relatively small inductance. However, a problem with the CPW structure becomes apparent in the implementation of some basic circuits, at mm-wave frequencies, such as the short circuited stub [4] which can exhibit ill-defined reflection coefficient curves — possibly due to the generation of surface waves. The problem is compounded by the high insertion loss at frequencies above 200 GHz and the related difficulty of achieving wide impedance ranges [5, 6]. Elevated CPW has been proposed to overcome the problem of implementing high impedance CPW transmission lines [7, 8]. The behavior of $50\,\Omega$ ECPW line has also been investigated up to 220 GHz [4]. A low dielectric constant and partial isolation from the semiconducting substrate can be achieved using ECPW. However, the performance of ECPW lines for typical lateral dimensions is observed to degrade rapidly at frequencies above approximately 240 GHz. This is possibly due to the non-complete isolation of the CPW traces from the substrate as there is still considerable penetration of the substrate by the electric field. To overcome this problem, a new variant of elevated CPW (referred to as GECPW) is presented. In this structure, a ground plane is placed on top of the substrate to provide near-complete isolation of the elevated CPW traces from the substrate. The electrical isolation of the signal trace from the bottom ground is achieved by the use of supporting posts in physical contact with the substrate via exposed rectangular areas in the lower ground plane bond pad layer. In fact, these are the only areas in which the line has direct physical contact with the substrate and in which dielectric loss is likely to occur. The structure provides a transmission line with much reduced dielectric loss and with very low loss per unit length in the 0 to 320 GHz frequency range.

   The paper first presents an approximate synthesis technique for the grounded elevated CPW (GECPW) portion of the line by building on previously established conformal mapping results and also presents some new analysis results for the post sections. The feed/post/line combinations in a real GECPW structures can be approximated as cascaded transmission lines with different characteristic impedances and effective dielectric constants [9]. Despite the effects associated with the discontinuities at the junctions of these different sections not
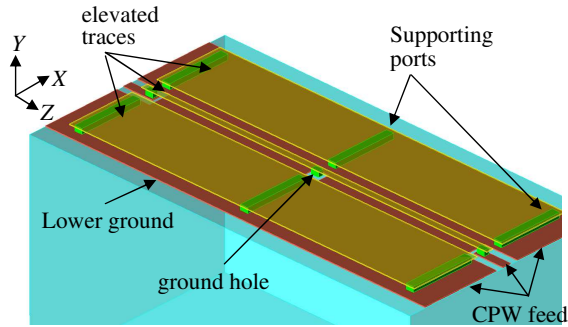
Figure 1. Angled 3-D conceptual view of a section of a grounded elevated CPW line resting on posts and fed by CPW.

being considered, good agreement between this semi-analytic approach and more comprehensive simulation results is achieved up to low mm-wave frequencies. The paper also presents measured examples of typical insertion losses of the new structure and CPW — the latter results comparing well with independently published results. The paper continues with the measured performance of several GECPW circuit components short and open-circuited matching networks and band-pass and band-stop filters with 6 μm and 13 μm elevation heights. CPW counterparts of all the circuits are also measured and their performance compared with that of the circuits implemented using the new transmission line topology.

2. GECPW ANALYSIS

2.1. Introduction to Grounded Elevated CPW

Figure 1 shows an example of a grounded elevated CPW transmission line along with posts and CPW feed sections. The CPW traces are suspended in the air above the substrate, post sections are used to connect the elevated traces to CPW feed lines and there is one supporting post section in the middle of the line with an area of substrate exposed.

The cross section of the elevated part of the line is simplified as shown in Figure 2. The CPW ground planes are assumed to be infinite in extent and the line is assumed to extend to infinity in the z-direction. The assumption of CPW ground planes of infinite extent yields accurate analysis results as long as the ground plane width does not become comparable with the quantity $2b$.
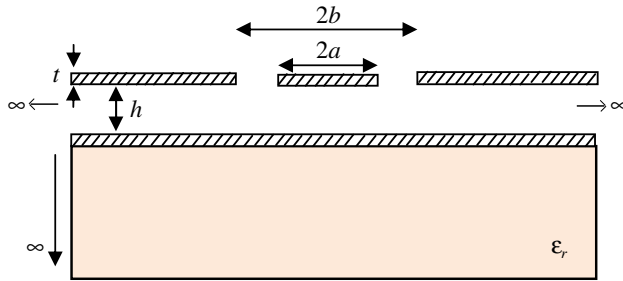
Figure 2. Cross section of the elevated grounded CPW.

2.2. Synthesis of Thick Elevated Grounded CPW Resting on Dielectric Substrate

The elevated grounded structure is essentially conductor-backed CPW with air as a substrate — see Figure 2. The quasi-TEM analysis of this structure has been reported by Ghione and Naldi [10]. However, the utility of this analysis is limited when the elevation becomes equal to or less than the gap width. The assumption of magnetic walls in the CPW slots is no longer valid as the top face of the CPW signal line couples to the ground plane beneath. In order to synthesize a grounded elevated CPW line with a specified capacitance, we consider three different ranges of parameter values:

$(b - a) < h$ — conductor backed CPW;

$h < (b - a) < 5h$ — combination of microstrip and conductor backed CPW;

$(b - a) > 5h$ — microstrip.

When $(b - a) < h$, the line can be synthesized by first finding the total line capacitance corresponding to the required characteristic impedance:

$$C_t = \frac{1}{cZ_0} \tag{1}$$

in which c is the speed of light in a vacuum. Next, we express the total line capacitance in terms of the contribution of the upper and lower half planes and an extra term representing the parallel plate capacitance between the signal and ground conductors formed by the finite metallization thickness. This is equivalent to introducing magnetic walls linking the top and bottom faces of the signal and ground lines. This simplifying assumption introduces some error into the computation but, in the range of practical line geometries, as will be shown, this error is relatively small. Specifically, the upper and lower

half plane capacitances are expressed in terms of elliptical integrals with modulus equal to $\frac{\tanh(\frac{\pi a}{2h})}{\tanh(\frac{\pi b}{2h})}$ and $\frac{a}{b}$ respectively. The parallel plate term is proportional to $\frac{t}{b-a}$. We now use the approximations [11] for K/K' when $0.707 < k < 1$ and when $0 < k < 0.707$ for the lower and upper half plane respectively and apply the Newton-Raphson method to obtain an iteration equation for b in terms of a and h:

$$b_{n+1} = b_n - \frac{\frac{t}{b_n-a} + \frac{\pi}{\ln(f)} + \frac{\ln(f_1)}{\pi} - \frac{C_t}{2\epsilon_0}}{\frac{\sinh(\frac{a\pi}{h})}{h(\cosh(\frac{a\pi}{h})-\cosh\frac{b_n\pi}{h})} - \frac{2\pi}{\sqrt{1-\frac{a^2}{b_n^2}}b_n\ln(f)^2} - \frac{t}{(a-b_n)^2}} \tag{2}$$

with

$$f = \frac{-4a^2 + 8\left(1 + \sqrt{1 - \frac{a^2}{b_n^2}}\right)b_n^2}{a^2} \tag{3}$$

$$f_1 = -4\mathrm{csch}\left(\frac{(a-b_n)\pi}{2h}\right)\sinh\left(\frac{(a+b_n)\pi}{2h}\right) \tag{4}$$

An initial value of $b = 1.5a$ yields, in most cases, accurate results for b in two to four iterations. When $(b - a) > 5h$, microstrip synthesis equations can be used [12]. However, when $h < (b - a) < 5h$ — the condition satisfied by a large range of practical GECPW geometries — using either of the above set of equations leads to large errors. In this case, for synthesis purposes, the total capacitance can be approximated as a combination of the above analysis — essentially grounded CPW empirically modified to reflect the coupling between the top face of the signal line and the bottom ground plane. The total line capacitance is now:

$$C_t = C_1 + (C_{ms} - C_2) + 0.9\varepsilon_0\frac{2a}{h} + C_{pp} \tag{5}$$

With the microstrip capacitance denoted C_{ms} and with C_1 and C_2 being the CPW and conductor backed CPW half plane capacitances respectively. The utility of separating the analysis into the three sets of simple equations is that an exact quasi-static solution of the structure involving multiple unknowns (the parameter problem) is avoided and yet accuracy good enough for design work is achieved. C_{ms} includes the effect of metallization thickness and can be calculated as per [13]. In a similar way to that used in deriving (2)–(4), we can obtain an iteration equation for b with assumed values of a, h and Z_0. The equation is:

$$b_{n+1} = b_n - \frac{2\epsilon_0\frac{\pi}{\ln(f)} - 0.63662\epsilon_0\frac{\ln(f_1)}{\pi} - C_t + C_{ms} + 0.9\varepsilon_0\frac{2a}{h}}{2\epsilon_0\left(\frac{-\coth\left(\frac{(a-b_n)\pi}{2h}\right)-\coth\left(\frac{(a+b_n)\pi}{2h}\right)}{2h} - \frac{2\pi}{\sqrt{1-\frac{a^2}{b^2}}b_n\ln(f)^2}\right)} \tag{6}$$

Table 1. Comparison between measured, calculated and simulated characteristic impedance for various geometries.

a	t	h	b	$Z_0\,(\Omega)$	Sim. $Z_0\,(\Omega)$
5	2	5	6.74	50	49.295
10	2	7	14.4	75	74.31
10	3	10	14.64	60	58.87
5	1	2	9.28	45	44.79
10	2	4	18.55	45	44.81
10	2	8	25.5	70	70.54
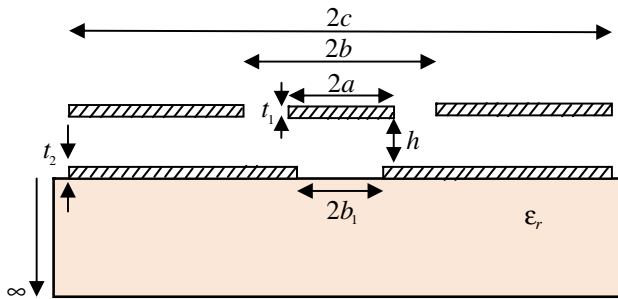
Figure 3. Cross section of a grounded elevated CPW section with gap on the lower ground.

Table 1 shows the desired characteristic impedance, the corresponding calculated dimensions and the impedance obtained from simulation results of a line with these dimensions. The results show that the synthesis formulae yield results with less than 1.9% error for the whole of the considered range.

2.3. Analysis of Thick Elevated Grounded CPW Resting on Dielectric Substrate with the Gap in Bottom Ground

A cross section of the part of the line which forms the transition between the elevated section and the section in which the signal line comes into physical contact with the substrate is shown in Figure 3. Here, we assume magnetic walls in the slots of the CPW and use Figure 4 to formulate the mapping function. The points in the intermediate t-plane and final t'' are shown along with the relevant points in the z-plane.
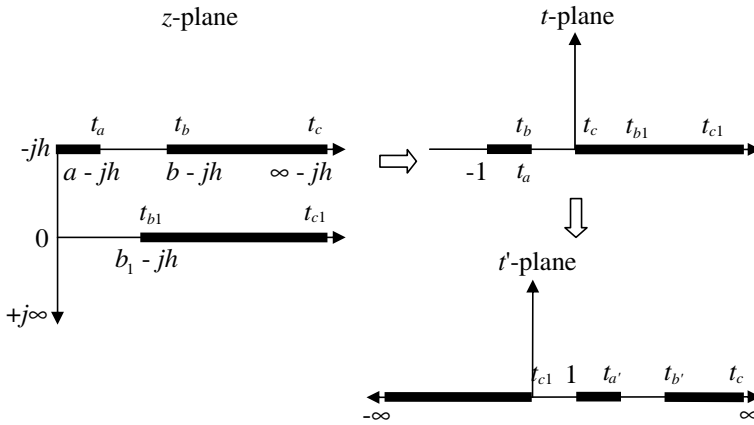
Figure 4. Mapping between physical (z) plane, intermediate t-plane and final t' plane for the intermediate post section.

The mapping function relating t and z-planes is

$$z = \frac{h}{t_{b1}\pi}\left(2\sqrt{t+1} + t_{b1}\log\left(\frac{1+\sqrt{t+1}}{-1+\sqrt{t+1}}\right)\right) \tag{7}$$

Setting $t = t_{b1}$, (7) involves only one unknown and allows us to numerically search for the value of t_{b1} which yields the known value of b on the left hand side. Once t_{b1} is known, left and right hand sides of the mapping function can be equated for each of the required z-plane points and the root of the equation solved using a suitable algorithm. With the t-plane points known, we further transform according to $t' = -\frac{1}{t}$. The elliptic modulus is now

$$K = \sqrt{\frac{\frac{t_a-1}{t_a}}{\frac{t_b-1}{t_b}}} \tag{8}$$

The resulting capacitance we denote C_3.

Finally, we use the series capacitance techniques in [14, 15] to find the total substrate capacitance for two layered substrates ordered in terms of decreasing permittivity as follows

$$C_4 = \frac{\frac{\epsilon_r}{\epsilon_r-1}C_2\epsilon_r C_3}{\frac{\epsilon_r}{\epsilon_r-1}C_2 + \epsilon_r C_3} \tag{9}$$

The total line capacitance can be written

$$C_{t1} = C_4 + C_1 + 2\epsilon_0\frac{t}{b-a} \tag{10}$$
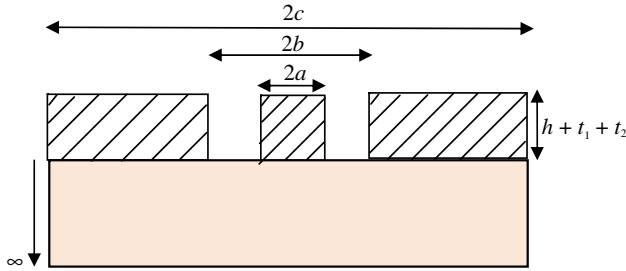
Figure 5. Cross section of GECPW post section.

2.4. Analysis of Post Section

The cross section of the region of the line in which the signal trace comes into contact with the substrate can be approximated as — or artificially forced to look like — CPW with thick metallization. With reference to Figure 5, the capacitance of this section can be approximated as the sum of the lower and upper CPW half plane capacitance and a parallel plate capacitance term proportional to $(h+t_1+t_2)/(b-a)$. Where t_1 and t_2 refer to the metallization thickness of the bond pad and airbridge layers respectively.

2.5. Quasi-static Characteristics of Composite Line

Figure 6 shows the results of a cascaded transmission line analysis when applied to a line characterized by a A/B/C/D/C/B/C/D/C/B/A geometry where A = CPW feed, B = post section, C = grounded CPW with gap in the ground plane and D = elevated grounded CPW. The parameters for the CPW section are $\varepsilon_{eff} = 6.186$, $Z_0 = 42.23\,\Omega$, $l = 20\,\mu\text{m}$. For the post section they are $\varepsilon_{eff} = 5.1318$, $Z_0 = 36.93\,\Omega$, $l = 22\,\mu\text{m}$. For the elevated section with gap on the lower ground, they are $\varepsilon_{eff} = 1.155$, $Z_0 = 104.387\,\Omega$, $l = 10\,\mu\text{m}$ and for the elevated section they are $\varepsilon_{eff} = 1$, $Z_0 = 87.7\,\Omega$, $l = 468\,\mu\text{m}$. Also shown are the results obtained from full wave solver Ansoft's HFSS$^{\text{TM}}$. All results assume infinite conductivity and zero dielectric loss.

It can be seen that the low frequency impedance is computed almost exactly whilst the high frequency dispersion is accurately modeled up to about 140 GHz in this particular case. A full wave analysis is required above this frequency to accurately compute the dispersion relation. Nevertheless, a quasi static analysis is useful in designing the post sections in order to reduce the effects of impedance mismatch in the line.
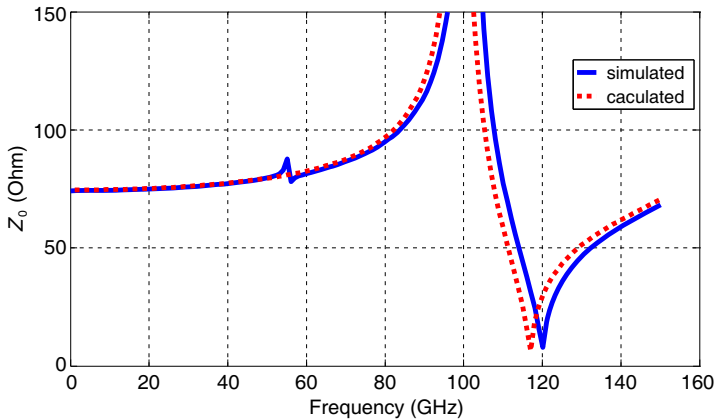
Figure 6. Comparison between simulated and calculated frequency dependent characteristic impedance for seven section line.

3. FABRICATION, MODELING AND MEASUREMENT

In order to realize the elevated structures, three fabrication steps were required. In the first step, the lower ground plane was defined by e-beam exposure and development of a $1.5\,\mu m$ thick layer of PMMA followed by electron beam evaporation and lift-off of a $50\,nm/1.2\,\mu m$ thick nichrome/gold layer. The second and third steps employ photolithography and electroplating techniques to form the suspended airbridge structures. The supporting posts for the elevated sections were formed by optical exposure and development of AZ4562 resist. The AZ4562 photoresist was spun with different speeds to achieve the desired thickness. The elevation height can be varied by defining this resist thickness. In our process, spinning AZ4562 at the speed of 3000 rpm for 30 s leads to a thickness of roughly 6–$6.5\,\mu m$. To achieve a greater thickness, this process can be repeated. After resist development, the metallization at this stage is achieved by evaporation of Ti/Au ($50\,nm/10\,nm$) followed by sputtering of $40\,nm$ gold to provide the electrical contact for the subsequent electroplating. In order to define the elevated tracks, $2\,\mu m$ thick S1818 photoresist was used followed by photolithography, development and ashing using a dry etch machine. The sample was then metalized using gold electroplating. Finally, different levels of exposure and development were performed to remove all the resist. Figure 7 shows the micrographs of a typical grounded elevated CPW line.

The GECPW passive components on $625\,\mu m$ GaAs substrate were simulated using Ansoft HFSS^{TM}, a 3-D full wave electromagnetic
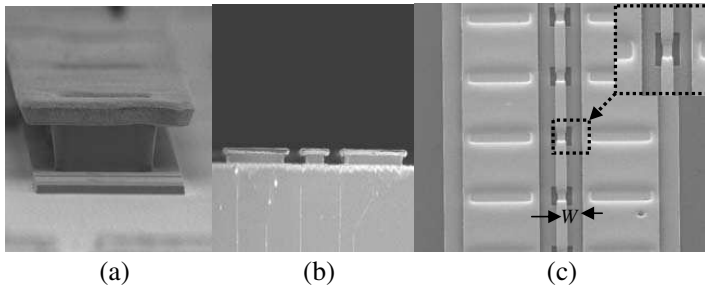
Figure 7. Micrograph of the grounded elevated CPW line at (a) post section, (b) cross sectional view and (c) top view.

simulation tool and Ansys Q3D, a 2D finite element solver. For the modeling, the following electrical parameter values were used: $1.2\,\mu\text{m}/2\,\mu\text{m}$ thicknesses for gold conductors, conductivity of $4.1 \times 10^7\,\text{S/m}$, 0.0016 for loss tangent and 12.9 for dielectric constant.

On-wafer S-parameter measurements were performed with an Agilent PNA network analyzer over the range 140–220 GHz and 220–320 GHz (G and H-band) using $50\,\mu\text{m}$-pitch WR-05 and WR-03 waveguide probes and 10 MHz–110 GHz using $100\,\mu\text{mm}$-pitch probes. The system was calibrated using the SOLT method with alumina ISS standards placed on an absorbing material. We checked the validity of the SOLT calibration through the measurement of long CPW lines on the ISS calibration substrate which were compared with careful EM simulations. Also, the results were compared with those obtained from a TRL calibration. The two results were essentially identical but those from the SOLT calibration were smoother and so these were used in subsequent analysis. The reference planes for the measurements were placed at the probe tips. To ensure the correct placement of the reference planes in all frequency bands, we checked that the phase of S_{21} was continuous at the cross-over frequencies. The samples were placed on thick quartz during the measurements. The Quartz spacer is used to eliminate any possible microstrip-like mode caused by the metal chuck from propagating.

4. GROUNDED ELEVATED CPW PASSIVE COMPONENTS

4.1. Transmission Line

In this section, the attenuation characteristics of the grounded elevated CPW line are investigated by comparing measured data for GECPW

lines with that for conventional CPW lines. At low frequencies, the dominant loss mechanism of the CPW line is that due to the finite conductivity of the metallization. At higher frequencies (dependent on the particular lateral dimensions used and the substrate parameters) the losses are dominated by those due to radiation. However, the radiation losses are due mainly to the very presence of a high dielectric constant substrate. Across the whole range of frequencies of interest, the substrate $(\tan \delta)$ losses remain relatively low for a GaAs dielectric. Measured results indicate that, at low frequencies, where the substrate and radiation losses are relatively small and
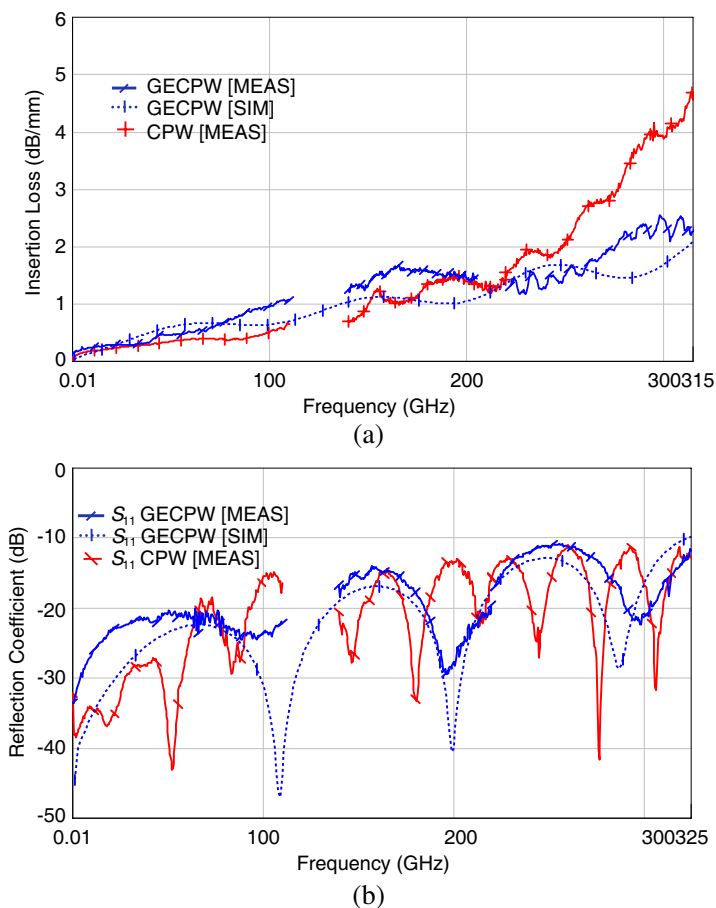
Figure 8. Measured and simulated S-parameters for a GECPW and CPW. (a) Insertion loss per mm. (b) Reflection Coefficient (dB).

attenuation is dominated by conductor loss, the attenuation of the
CPW and GECPW lines are roughly comparable. However, at
high frequencies (above approximately 200 GHz for these particular
CPW lateral dimensions), when the radiation and substrate losses of
CPW become significant, the GECPW line gains an advantage. The
GECPW line, unlike a conventional CPW line, is isolated from the
substrate, has essentially zero dielectric loss and does not radiate to
any significant extent. The post and feed sections, however, do have
losses of these types but because the majority of the physical extent of
the line consists of elevated sections, the overall losses are reduced.

Figure 8 shows the measurement and simulation results for a
line with a nominal impedance of $54\,\Omega$ and dimensions of signal
width $(W) = 24\,\mu\mathrm{m}$, gap width $(S) = 25\,\mu\mathrm{m}$ and ground width
$(Wg) = 105\,\mu\mathrm{m}$. GECPW transmission line along with the results
of conventional CPW for comparison. For this measurement, probing
was done on top of the elevated traces by placing two post sections
close together to make a stable landing pad.

It can be seen that, by using a grounded elevated CPW structure,
improvements in the line performance in terms of loss/mm over a
conventional CPW line can be achieved — especially at frequencies
above 200 GHz. The CPW attenuation results were compared with
those of [16, 17] and are in very close agreement, validating the
measurement process.

4.2. Transition to Coplanar waveguide

Elevated CPW lines cannot be suspended in air over their entire length
but must include post and feed sections — not only for mechanical
reasons but so they can be connected to transistors and/or passive
components. In Figure 9, measurements for a GECPW line with
transitions to CPW are compared with the results of a line with de-
embedded transition.

Figure 9 clearly shows the deleterious effect of the transition
pad on the performance of GECPW line. Comparing the measured
insertion loss for the GECPW line in Figure 8(a) with that of Figure 9
it can be seen that the two methods of removing the effect of the
transition are in close agreement. Moreover, the effect shown in
Figure 9 in the measured GECPW line without de-embedding and
the CPW line — that of a sudden increase in attenuation above
210 GHz — is shown to disappear using both techniques. The effect
of the transition on the overall performance of grounded elevated
CPW becomes more significant at the frequencies for which CPW
degradation is more pronounced. The de-embedded grounded elevated
CPW line shows very low loss/mm at high mm-wave regimes — almost
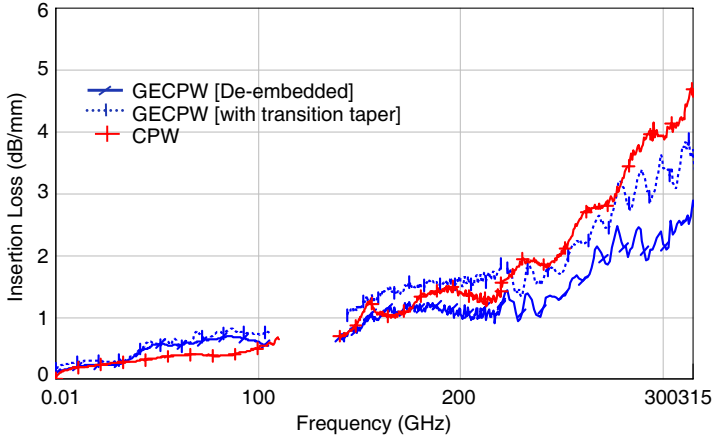
Figure 9. Measured *S*-parameters for a tapered GECPW, de-embedded GECPW and CPW transmission lines insertion loss/mm.

half the loss for the CPW line with the same characteristic impedance. Note that a rigorous optimization has not been conducted in the design of the CPW transitions and our design is based on a simple matching of quasi-static characteristic impedances.

Some aspects of the discussed measurement results deserve further comment. The wavelength in the GECPW with air dielectric is longer than in a CPW line with GaAs dielectric. Measured results for the CPW line reveal that the loss, in dB per *wavelength*, at 260 GHz, is about $1.3\,\mathrm{dB}/\lambda g$ whilst for the GECPW line the figure is $1.6\,\mathrm{dB}/\lambda g$. The same measurement at 70 GHz shows $1.9\,\mathrm{dB}/\lambda g$ for CPW line while $1.6\,\mathrm{dB}/\lambda g$ is observed for GECPW. These results show that, in terms of loss per wavelength and considering the effects of measurement error, the two lines are broadly comparable over the d.c. — 320 GHz range but also that, for a fixed length, the GECPW line exhibits considerably less loss. The real advantage of the GECPW structure over conventional and previously reported elevated CPW structures is that low loss transmission lines within a wide impedance range of $5\,\Omega$–$100\,\Omega$ can easily be achieved by varying the elevation above the substrate. In contrast, CPW transmission line cannot satisfactorily implement such extremes of characteristic impedance due to excessive losses [5]. Also, previously reported elevated structures tend only to support higher impedances with reasonable dimensions. The ability to easily implement high and low impedances with GECPW lines of reasonable dimensions can therefore be considered a great advantage.

Besides, in CPW and other previously reported elevated-CPW

structures, small lateral dimensions $(W + 2S)$ are required to achieve low radiation losses at mm-wave frequencies. In contrast, the radiation loss mechanism of the GECPW structure is, to a large extent, independent of the lateral dimension. When the limitations of the fabrication process are considered, it can be advantageous to avoid especially small gaps or signal widths such as are required to achieve low and high impedance lines in conventional CPW. Further advantages are found in the design of passive circuit components such as the matching stubs and filters described in following sections.

The results presented here suggest that grounded elevated CPW has a performance comparable with conventional CPW at lower frequencies. Furthermore, the absence of high attenuation well into
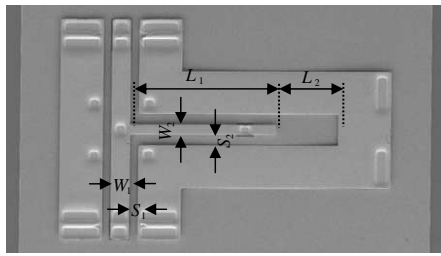
Figure 10. Micrograph of open circuited stub. The stub dimensions are $L_1 = 350$, $L_2 = 145$, $S_1 = 19.5$, $S_2 = 26$, $W_1 = 45$, and $W_2 = 23.5$. All dimensions are in microns.
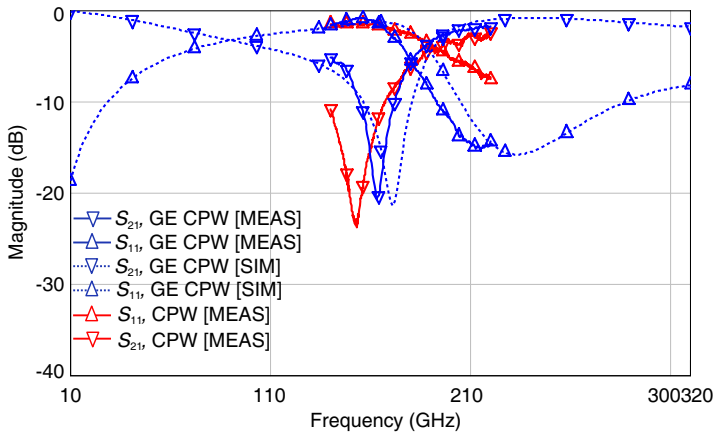
Figure 11. Measured and simulated S-parameters for a GE CPW open-end shunt stub.

the sub-millimeter wave frequencies suggest reduced dielectric-related loss.

4.3. Open Circuit Matching Network

One of the coplanar waveguide components whose performance can be improved is the open circuited matching network. To study the performance of the open circuit stub using grounded elevated CPW, a series of open circuited 90° shunt stubs were designed and fabricated with different center frequencies. A micrograph of an implemented GECPW matching network incorporating an open circuited stub is shown in Figure 10.

To demonstrate the stub characteristics, a comparison between the measured and modeled characteristics of a matching network using GECPW and the measured results of one implemented using CPW is given in Figure 11. The GECPW network shows an in-band-loss at the 90° frequency (163 GHz) of the stub of 0.9 dB and a 3 dB-bandwidth of 100 GHz. The CPW open stub shows an in-band-loss of 1.58 dB at the frequency of 153 GHz and a 3 dB-bandwidth of 112 GHz. This is a reduction in loss of around 0.7 dB.

To achieve optimum performance for the GECPW network we designed the shunt connected line to have a higher impedance than the series lines. However, even a non-optimized GECPW network measures superior performance with 1.2 dB insertion loss and a bandwidth of 105 GHz. Increasing the elevation height from 6 μm to 13 μm yielded an in-band-loss of 1 dB at 149 GHz with a bandwidth of 100 GHz. This suggests that the performance of a GECPW open circuit stub is fairly insensitive to elevation height. However, lower elevation is advantageous in terms of yield and fabrication complexity.
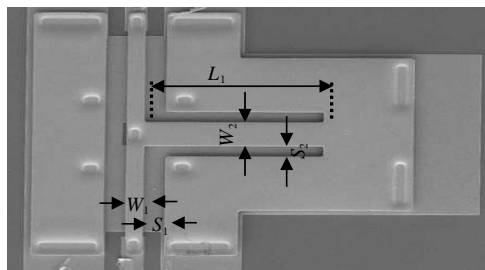
Figure 12. Micrograph of short circuited stub. The stub dimensions are $L_1 = 251$, $S_1 = 30$, $W_1 = 24$, $S_2 = 19.5$ and $W_2 = 44.8$. All dimensions are in microns.
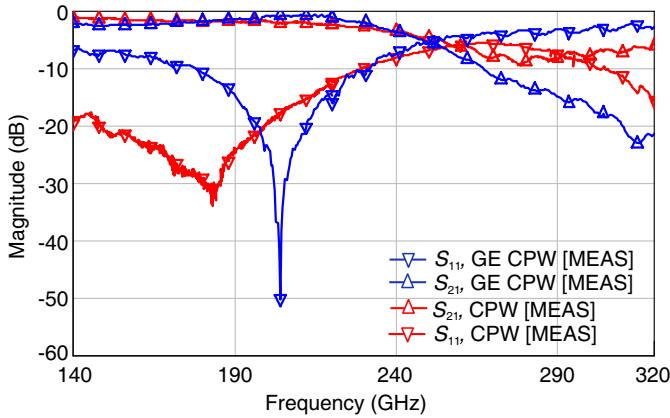
Figure 13. Measured S-parameters for GECPW short-end shunt stub with $13\,\mu\text{m}$ elevation.

4.4. Short Circuit Matching Network

The short circuited shunt stub matching network, is a useful topology for a variety of circuits including band-pass filters, diode detectors and matching/dc return networks. Figure 12 is a micrograph of such a network implemented using GECPW.

The performance of CPW short circuit matching stubs at high frequencies has been investigated [4]. Figure 13 shows some measured results for CPW and GECPW short circuited matching stubs. Due to unwanted substrate effects at high frequencies, the CPW short circuit stub designed for $240\,\text{GHz}$ exhibits a very large bandwidth and ripples in the reflection coefficient. The loss at the center frequency is $1.8\,\text{dB}$.

Simulation results for CPW short circuit stub show a similar effect at these frequencies. The grounded elevated CPW short circuited stub with a center frequency of $245\,\text{GHz}$ and at $6\,\mu\text{m}$ elevation exhibits $1.6\,\text{dB}$ in-band loss at the center frequency with better matching to $50\,\Omega$ than the CPW short circuit stub but the performance is not greatly enhanced. However, by increasing the elevation height to $13\,\mu\text{m}$, the performance of the short circuited GECPW matching stub is observed to improve drastically. Results for $13\,\mu\text{m}$ elevation along with those for a CPW stub resonating at a slightly lower frequency are shown in Figure 13.

In Figure 13, the GECPW stub shows $0.7\,\text{dB}$ loss at the center frequency of $204\,\text{GHz}$ compared with $1.8\,\text{dB}$ for CPW at the center frequency of $185\,\text{GHz}$.

Using a balanced shorted stub with $13\,\mu\text{m}$ elevation increases the

insertion loss at the center frequency to 1.35 dB and reduces the 3-dB bandwidth to 77 GHz. The increased loss in this case is mainly attributable to the increase in overall conductor loss.

In order to suppress the slotline mode at the discontinuities, additional supporting posts were used to connect the top and lower ground planes at the junctions. We tried stubs without these additional connecting posts and the response was very different from those shown in Figure 13. The bandwidth was much larger and the insertion loss was increased by at least 1.3 dB.
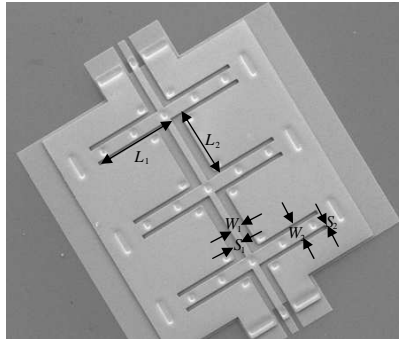
Figure 14. Micrograph of the 3rd order quarter-wavelength band-pass Filter. The filter dimensions are $L_1 = 270$, $L_2 = 252$, $S_1 = 37$, $S_2 = 14$, $W_1 = 21$, and $W_2 = 44.5$. All dimensions are in microns.
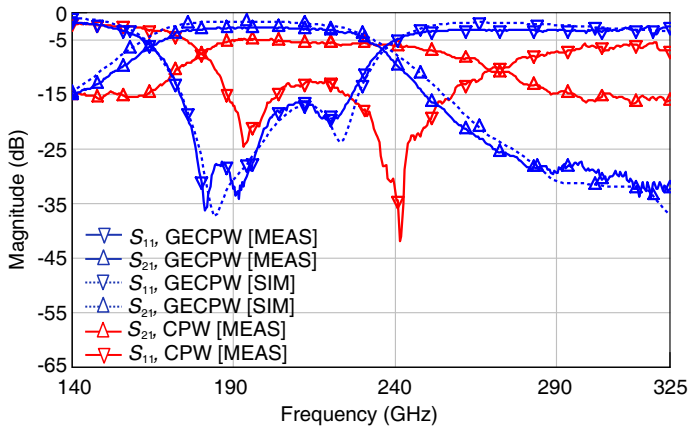
Figure 15. Measured and simulated S-parameters for a GE CPW band-pass filter.
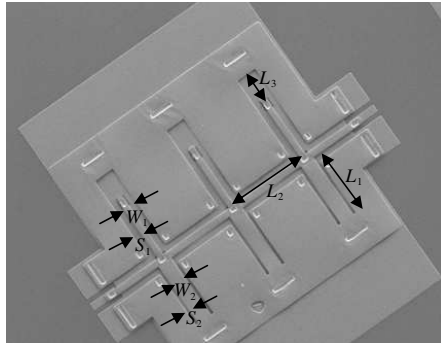
Figure 16. Micrograph the 3rd order quarter-wavelength band-stop Filter. The stub dimensions are $L_1 = 243$, $L_2 = 220$, $L_3 = 150$, $S_1 = 28$, $S_2 = 12.5$, $W_1 = 21$, and $W_2 = 51$. All dimensions are in microns.

4.5. Band-pass Filter

A third order quarter-wavelength band pass filter was designed by cascading 3 double short circuited stubs. Figure 14 shows a micrograph of the filter.

Using grounded elevated CPW with very low radiation and attenuation, results in very low passband insertion loss for filters. With reference to Figure 15, a GECPW 3rd-order band-pass filter with a center frequency of 200 GHz, has an insertion loss of 2.6 dB at the center frequency with a 3 dB-bandwidth of 66 GHz. Measurement/simulation results show very poor performance for the 3rd-order band-pass filter designed with CPW transmission media [18], with an insertion loss of 5.7 dB at the center frequency of 220 GHz and 3 dB-bandwidth of 93 GHz.

There is thus an advantage in using grounded elevated CPW for sub-millimeter wave transmission line-based filters over conventional CPW implementations. Also, increasing the elevation height from 6 μm to 13 μm reduces the insertion loss to 1.9 dB without significant change in the 3 dB-bandwidth (69 GHz).

4.6. Band-stop Filter

By cascading multiple open circuited shunt stubs, it is quite simple to realize a band stop filter with low in-band loss and high out-of-band frequency rejection. A third order quarter wavelength band-stop filter was designed and fabricated using a GECPW structure.

Using this circuit topology, however, did not yield performance
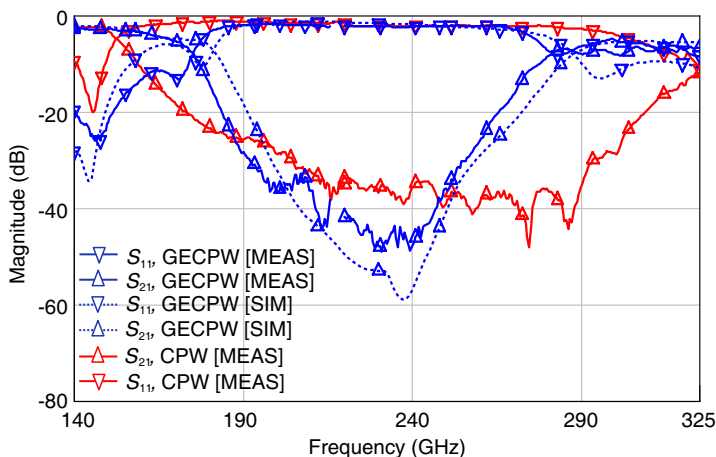
Figure 17. Measured and simulated S-parameters for a GECPW band-stop filter.

greatly superior to CPW. Therefore, a combination of short and open circuited shunt stubs was used to realize the band-stop filter, see Figure 16. This improved the performance of the filter with higher out-of-band attenuation and lower in-band loss.

With reference to Figure 17, the 3rd-order quarter-wavelength GECPW band stop filter shows 2.1 dB in-band loss at the center frequency of 230 GHz with a 3 dB bandwidth of 99 GHz. Compared with its CPW counterpart, the GECPW filter shows similar insertion loss but a 61 GHz reduction in the bandwidth. By increasing the elevation height from 6 μm to 13 μm, the in-band loss reduces to 1.5 dB while the 3 dB-bandwidth stays almost constant.

5. CONCLUSION

A new type of elevated CPW transmission line, Grounded elevated CPW (GECPW), has been shown to provide low insertion loss and low sensitivity to substrate effects at frequencies up to 320 GHz. Simple equations have been formulated to facilitate design work and show good agreement with simulation results and measurement. The MMIC compatible GECPW structure offers an extremely low insertion loss (2.5 dB/mm) at these frequencies which is almost 2.5 dB less than the insertion loss of an equivalent CPW line and 3.3 dB less than an elevated CPW line at the same frequency. Circuit components such as short and open circuited stubs, band-pass filters and band-stop

filters designed with the GECPW structure all show a performance enhancement compared with CPW counterparts up to 320 GHz. Two mm-wave band pass filters — one implemented with CPW and the other with GECPW — show that a decrease of 3.1 dB in loss can be achieved at the center frequency by using the new transmission line structure. This is a considerable reduction in pass-band loss and amply demonstrates the potential of the novel transmission line structure to enhance the performance of mm-wave circuits.

REFERENCES

1. Deal, W. R., X. B. Mei, V. Radisic, W. Yoshida, P. H. Liu, J. Uyeda, M. Barsky, T. Gaier, A. Fung, and R. Lai, "Demonstration of a S-MMIC LNA with 16-dB gain at 340 GHz," *IEEE Compound Semiconductor Integrated Circuit Symposium*, 1–4, 2007.

2. Mei, X. B., W. Yoshida, P. H. Liu, J. Uyeda, J. Wang, W. Liu, D. Li, Y. M. Kim, M. Lange, T. P. Chin, T. Gaier, A. Fung, L. Samoska, and R. Lai, "35-nm InP HEMT SMMIC amplifier with 4.4-dB gain at 308 GHz," *IEEE Electron. Device Letters*, Vol. 28, No. 6, Jun. 2007.

3. Tessmann, A., A. Leuther, H. Massler, V. Hurm, M. Kuri, M. Zink, M. Riessle, and R. Losch, "High-gain submillimeter-wave mHEMT amplifier MMICs," *Microwave Symposium Digest (MTT)*, 1, 2010.

4. Aghamoradi, F., I. McGregor, and K. Elgaid, "Performance enhancement of millimetre-wave resonators using elevated CPW," *Electron. Letters*, Vol. 45, No. 25, 1326–1328, Dec. 2009.

5. Jackson, R. W., "Considerations in the use of coplanar waveguide for millimetre-wave integrated circuits," *IEEE Trans. Microwave Theory Tech.*, Vol. 34, 1450–1456, Dec. 1986.

6. Weller, T. M., L. P. B. Katehi, and G. M. Rebeiz, "High performance microshield line components," *IEEE Trans. Microwave Theory Tech.*, Vol. 43, 534–543, Mar. 1995.

7. Schnieder, F., R. Doerner, and W. Heinrich, "High impedance coplanar waveguides with low attenuation," *IEEE Microwave Guided Wave Lett.*, Vol. 6, 117–119, Mar. 1996.

8. Kim, H. T., S. Jung, J. H. Park, C. W. Baek, Y. K. Kim, and Y. Kwon, "A new micromachined overlap CPW structure with low attenuation over wide impedance ranges," *IEEE Trans. Microwave Theory Tech.*, Vol. 49, No. 9, 2001.

9. McGregor, I., F. Aghamoradi, and K. Elgaid, "An approximate analytical model for the quasi-static parameters of elevated CPW lines," *IEEE Trans. Microwave Theory Tech.*, Vol. 58, 3809, Dec. 2010.

10. Ghione, G. and C. U. Naldi, "Co planar waveguides for MMIC applications: Effect of upper shielding, conductor backing, finite extent ground planes, and line-to-line coupling," *IEEE Trans. Microwave Theory Tech.*, 260–267, Vol. 35, 1987.

11. Hilberg, W., "From approximations to exact relations for characteristic impedances," *IEEE Trans. Microwave Theory Tech.*, Vol. 17, No. 5, 259–265, 1969.

12. Tang, W. C. and Y. L. Chow, "CAD formulas and their inverses for microstrip, CPW and conductor-backed CPW, by successive synthetic asymptotes," *Antennas and Propagation Society International Symposium*, Vol. 3, 394–397, 2001.

13. Chang, W. H., "Analytic IC-metal-line capacitance formulas," *IEEE Trans. Microwave Theory Tech.*, Vol. 24, 608–611, 1976; also Vol. 25, 712, 1977.

14. Ghione, G., M. Goana, G. L. Madonna, G. Omegna, M. Pirola, S. Bosso, D. Frassati, and A. Perasso, "Microwave modeling and characterization of thick coplanar waveguides on oxide-coated lithium niobate substrates for electrooptical applications," *IEEE Trans. Microwave Theory Tech.*, Vol. 47, No. 12, 2287–2293, 2002.

15. Ghione, G. and M. Goana, "Revisiting the partial-capacitance approach to the analysis of coplanar transmission lines on multilayered substrates," *IEEE Trans. Microwave Theory Tech.*, Vol. 51, No. 9, 2007–2014, 2003.

16. Cheng, H., J. F. Whitaker, T. M, and L. P. B. Katehi, "Terahetz-bandwidth characterzation of coplanar waveguide on dielectric membrane via time domain electro-optic sampling," *IEEE MTT-S International Microwave Symposium Digest*, Vol. 1, 477–480, 1994.

17. Zehentner, J. and J. Machac, "Properties of CPW in the sub-mm wave range and its potential to radiate," *IEEE MTT-S International Microwave Symposium Digest*, Vol. 2, 1061–1064, 2000.

18. Aghamoradi, F., I. McGregor, and K. Elgaid, "H-band elevated CPW band-pass filters on GaAs substrate," *Microwave Conference (EuMC)*, 9–12, 2010.